

Bormin Huang*, Alok Ahuja, Y. Sriraja and Hung-Lung Huang
CIMSS, University of Wisconsin-Madison

Mitchell D. Goldberg
NOAA, National Environmental Satellite, Data, and Information Service

1. INTRODUCTION

In the era of contemporary and future ultraspectral sounders (e.g. AIRS (Aumann et al. 2001), CrIS (Bloom 2001), IASI (Phulpin et al. 2002), GIFTS (Smith et al. 2002), HES (Huang et al. 2003) etc.), better inference of atmospheric, cloud, and surface parameters is feasible for improved weather forecast and climate prediction. Given the large volume of three-dimensional data generated by an ultraspectral sounder each day, the use of robust data compression techniques will be beneficial for data transfer and archival. The physical retrieval of these geophysical parameters, involving the inverse solution of the radiative transfer equation, is a mathematically ill-posed problem (Huang et al. 2002), i.e. the solution is sensitive to the error or noise in the data. Therefore, there is a need for lossless or near-lossless compression of ultraspectral sounder data to avoid potential retrieval degradation of meteorological parameters due to lossy compression.

In this paper we present a systematic study of various 2D and 3D lossless compression techniques for the next-generation NOAA GOES-R Hyperspectral Environmental Suite (HES). These techniques are divided into transform-based, prediction-based, projection-based, and clustering-based methods. The ultraspectral sounder data features strong correlations in disjoint spectral regions affected by the same type of absorbing gases at various altitudes. To take advantage of this feature, a bias-adjusted reordering (BAR) data preprocessing scheme (Huang et al. 2004b, Huang et al. 2005c) is used to improve compression gains of these state-of-the-art transform-based and prediction-based methods for ultraspectral sounder data. The minimum spanning tree (MST) reordering is also investigated. This paper also shows newly-developed compression schemes such as Lossless Multiwavelet Compression, Lossless Principal Component Analysis (Lossless PCA) (Huang et al. 2005c), Optimized Orthogonal Matching Pursuit (OOMP) (Rebello-Neira et al. 2002) based linear prediction, Predictive Partitioned Vector Quantization (PPVQ) (Huang et al. 2004a), and Fast Precomputed Vector Quantization (FPVQ) (Huang et al. 2005a) with optimal bit allocation, that all yield significantly higher compression ratios on ultraspectral sounder data than state-of-the-art compression schemes (e.g. JPEG2000,

JPEG-LS and CALIC). Furthermore, an error-robust data compression technique using reversible variable-length codes (RVLCs) is presented. Results show that RVLCs performs significantly better error containment than JPEG2000 Part 2 on the standard ultraspectral sounder data set.

The rest of the paper is arranged as follows. Section 2 describes the ultraspectral sounder data used in this study. Section 3 highlights the data preprocessing schemes, while Section 4 elaborates the various compression schemes. Section 5 summarizes the paper.

2. DATA

The ultraspectral sounder data could be generated from either a Michelson interferometer (e.g. CrIS, IASI and GIFTS) or a grating spectrometer (e.g. AIRS). The ultraspectral sounder data set with 2107 AIRS channels was prepared at the direction of NOAA to serve as a standard test set for ultraspectral sounder data compression studies. The data is publicly available via anonymous ftp (<ftp://ftp.ssec.wisc.edu/pub/bormin/Count>). It consists of 10 digital count granules, five daytime and five nighttime, selected from representative geographical regions of the Earth. Their locations, UTC times and local time adjustments are listed in Table 1.

This standard ultraspectral sounder data set is obtained from NASA AIRS digital counts collected on March 2, 2004. The AIRS data includes 2378 infrared channels in the 3.74 to 15.4 μm region of the spectrum. A day's worth of AIRS data is divided into 240 granules, each of 6 minute durations. The AIRS digital count data ranges from 12-14 bits for different channels. More information regarding the AIRS instrument may be acquired from the NASA AIRS website (<http://www.airs.nasa.jpl.gov>). To make the selected data more generic to other ultraspectral sounders, 271 bad channels identified in the supplied AIRS infrared channel properties file are excluded, assuming that they occur only in the AIRS sounder. Each resulting granule is saved as a binary file, arranged as 2107 channels, 135 scan lines, and 90 cross-track footprints per scan line, i.e. there are a total of $135 \times 90 = 12,150$ footprints per channel. Figure 1 shows the AIRS digital counts at wavenumber 800.01cm^{-1} for the 10 selected granules on March 2, 2004. In these granules, coast lines are depicted by solid curves, and multiple clouds at various altitudes are shown as different shades of colored pixels.

*Corresponding author address: Bormin Huang,
1225 W. Dayton St., Madison, WI 53706;
e-mail: bormin@ssec.wisc.edu

3. DATA PREPROCESSING SCHEMES

Ultraspectral sounder data features strong correlations in disjoint spectral regions due to the same type of absorbing gases. Figure 2 shows an example of the dominant absorbing gases in different spectral regions.

Bias Adjusted Reordering: The Bias-Adjusted Reordering (BAR) scheme (Huang et al. 2004b) takes advantage of the aforementioned spectroscopic characteristic of ultraspectral sounder data. When combined with a 3D compression scheme (e.g. 3D SPIHT (Tang et al. 2003, Said et al. 1996)), the BAR scheme reorders the spectral channels, each of which corresponds to a 2D spatial frame. It exploits the spectral correlations among disjoint channels resulting in compression gains. When the BAR scheme is combined with a 2D compression scheme (e.g. 2D JPEG2000 (ISO/IEC 2000), 2D JPEG-LS (ISO/IEC 1999), 2D CALIC (Wu 1997)), the 3D sounder data is first made two-dimensional by converting the two spatial dimensions into one dimension via a continuous scan (e.g. horizontal, vertical and diagonal zigzag scans, Peano scan (Yang et al. 1988) that smoothens the transition of data samples from one line to another. The BAR scheme is then applied along the spectral and/or spatial dimension. In doing so, it can exploit the spectral correlations among disjoint channels, and/or the spatial correlations of disjoint geographical regions affected by the same type of absorbing gases or clouds.

The effects of the BAR scheme can be gauged by looking at the reordered 2D data patterns in the spectral-spatial domain. Figure 3 shows such an example for granule 82. Comparing Fig. 3(a) with Fig. 3(b), we can see that the data pattern is smoother along the spectral dimension after spectral reordering. This results in a higher compression ratio for Fig. 3(b). Similarly, the spatially reordered data in Fig. 3(c) is smoother than the data in Fig. 3(a) along the spatial dimension. Fig 3(d) depicts the reordering along both dimensions that produces a smoother transition along both dimensions. Moreover, the bias adjustment reduces the dynamic range of the reordered data as visualized by the reduction of colored intensities. Following the BAR preprocessing, significant compression gains have been reported on 3D SPIHT, 2D JPEG2000, 2D JPEG-LS and 2D CALIC in (Huang et al. 2005b, Huang et al. 2005c).

Figure 4 shows the sorted indices plotted against the original indices in the cases of spectral BAR for four granules. The sorted indices are quite different from the original indices as judged by their great deviation from the straight line. This shows that the natural channel ordering by the spectral wavelengths does not possess optimal correlation in neighboring channels. In the BAR scheme, a given starting channel produces its own unique list of reordering indices. Subsequently, the compression ratios are different for the BAR scheme using different starting channels. An investigation of the effects of the starting channel was conducted by Huang et al. (2004c). It was shown that any starting channel

could be used without compromising the compression ratio significantly for the ultraspectral sounder data.

Minimum Spanning Tree Reordering: An optimal ordering of the channels can also be obtained using the Minimum Spanning Tree (MST) (Cormen et al. 2001). Previous work (Tate 1997; Toivanen et al. 2005; Kubasova et al. 2004) used MST with various cost functions to find optimal ordering of bands for prediction. For lossless compression of ultraspectral sounder data, we explored MST reordering followed by arithmetic coding (AC) (Witten et al. 1987) of the prediction residuals. Table 2 depicts the compression ratios for the standard ultraspectral sounder data set obtained using MST reordering with both context-free and context-based arithmetic coding. For comparison, the compression ratios using spectral BAR preprocessing are also listed. As seen, MST reordering with context-free AC produces a higher average compression ratio than its spectral BAR counterpart. On the other hand, BAR is better than MST with context-based AC.

4. COMPRESSION SCHEMES

4.1 Transform-based schemes

3D SPIHT with BAR: SPIHT (Said et al. 1996) is an embedded coding algorithm that performs bit-plane coding of the wavelet coefficients. It uses spatially oriented trees to describe the relationship between the parents on higher levels to the children and grandchildren on lower levels. It has low complexity and provides good performance. Extensions to 3D have been proposed in (Tang et al. 2003; Dragotti et al. 2000). Huang et al. (2003) presented a 3D SPIHT version to tackle irregular size 3D data, the dimensions of which need not be divisible by 2^N , where N is the levels of wavelet decomposition being performed. For application to ultraspectral sounder data, various 3D integer wavelet transforms were used followed by the 3D SPIHT method and arithmetic coding. The compression ratios obtained are shown in Fig. 5. As can be seen, different choices of wavelet transforms produce different compression ratios. The compression gains using the spectral BAR preprocessing are evident in Fig. 6. The compression ratios obtained for all ten granules are significantly higher with spectral BAR followed by 3D SPIHT than using 3D SPIHT alone.

JPEG2000 with BAR: This algorithm is published as a new standard of ISO/IEC, as well as an ITU-T recommendation (ISO/IEC 2000a). Its rich feature list includes progressive transmission by quality, resolution, component, or spatial locality, lossy and lossless compression, region of interest coding by progression, and limited memory implementations, to name a few. The JPEG2000 encoder consists of four main stages: discrete wavelet transform (DWT), scalar quantization, and two tiers of block coding, as depicted in Fig. 7. After the DWT stage, embedded scalar quantization is performed with the quantization step size possibly varying for each subband. The block coder is based on

the principles of Embedded Block Coding with Optimized Truncation (EBCOT) (Taubman 2000) and includes an arithmetic coder coupled with a rate-distortion optimization algorithm to achieve the optimal bit rates. The performance of JPEG2000 compression with and without the BAR preprocessing scheme applied along spectral and/or spatial dimension on the ten granules is shown in Fig. 8. As can be seen in the figure, BAR significantly improves JPEG2000 compression gains.

Lossless Multiwavelet Compression with BAR: Multiwavelets (MWT) are different from wavelets in that they have more than one scaling and wavelet functions. Multiwavelets are theoretically expected to perform better than traditional wavelets for image compression applications (Martin 2001). We create a 2D representation of the 3D sounder data and perform multiwavelet decomposition. The multiwavelet decomposition data is then presented to a context-based arithmetic coder to achieve lossless compression. To achieve lossless compression using MWT, a reversible integer-to-integer implementation of the MWT is performed. This implementation is obtained based on the lifting steps for MWT given by Cheung et al. (Cheung 1999), and uses the integer Haar transform for both the pre-filter and the transform steps. The different subbands are extracted from the multiwavelet representation and presented individually to the arithmetic coder for lossless compression. The arithmetic encoder is able to find more contexts within the coefficients of each subband and is able to provide a better compression performance. The compression results for all the ten granules with and without BAR preprocessing are shown in Figure 9. It can be seen that on an average the use of BAR pre-processing improves the compression ratio by about 15%.

3D Wavelet Transform with Reversible Variable-Length Coding: Nonreversible variable-length codes (e.g. Huffman coding (Huffman 1952), Golomb-Rice coding (Golomb 1966; Rice 1979), and arithmetic coding (Said 2004)) have been conventionally used to increase compression efficiency. However, these are very vulnerable to error occurrence during noisy transmission of compressed bit-streams. A single bit-error is most likely to propagate such that many subsequent codewords are misinterpreted by the decoder leading to substantial degradation of the original data source. Reversible variable-length codes (RVLCs) (Takishima et al. 1995) offer a solution to this problem by providing greater error robustness than their nonreversible counterparts. RVLCs can be decoded in both the forward and backward direction, allowing 'recovery' of large parts of the corrupted bit-stream that would have been lost in a nonreversible variable length-code. This has led to the adoption of RVLCs in the latest video coding standards of MPEG-4, H.263+, H.263++ (ISO/IEC 1998; ITU-T 1995). Huang et al. (2005d) investigated RVLCs for lossless compression of ultraspectral sounder data. In their proposed scheme, a 3D integer wavelet transform (3DWT) is first performed

on the ultraspectral sounder data. Blocks of wavelet coefficients are then grouped together and entropy coded using RVLCs. The standard ultraspectral sounder data set is compressed using both schemes of 3DWT+RVLC and JPEG2000 Part 2 (ISO/IEC 2000b). Table 3 shows lossless compression ratios for the ten tested granules using JPEG2000 Part 2 (3DWT+MQ arithmetic coder) and 3DWT+RVLC. The error resilient mechanism of JPEG2000 (Taubman et al. 2002) is utilized to encode the granules. As seen from Table 3, the average compression ratio produced by 3DWT+RVLC is only 4.2% lower than that of JPEG2000 Part 2. To investigate the error-resilience capabilities of both schemes for an erroneous bit survived from channel decoding, a single bit is randomly flipped in each compressed granule, and the original and decompressed granules are compared to determine the number of pixel errors. The propagation of the single bit-error after source decoding greatly depends on the specific 3DWT resolution in which the bit-error occurs. Therefore, 30 events of randomly flipping a single bit are simulated for each of the 6 spectral and 4 spatial resolutions in all compressed granules. The number of incorrectly decoded pixels is then determined by comparing the original and decompressed granules. Figure 10 depicts the average number of pixels errors for 30 events in 24 resolutions for ten granules. A bit error in a lower resolution generally produces a much larger number of pixel errors than those produced in a higher resolution. Furthermore, 3DWT+RVLC produces significantly fewer number of pixel errors than JPEG2000 for all resolutions in the ten granules.

4.2 Prediction-based schemes

CALIC with BAR: The CALIC scheme (Wu 1997) is considered as the most efficient and complex encoder for compression of 2D continuous-tone images. Among the nine proposals in the initial ISO/JPEG evaluation in July 1995, CALIC was ranked first. It works on the principle of a context-adaptive non-linear predictor which adjusts to the local gradients around the current pixel. As shown in Fig. 11, the algorithm operates in the binary or continuous modes. The binary mode codes those regions of the image where the intensity values are less than two. In the continuous mode, the system has four major components: gradient-adjusted prediction, context selection and quantization, context modeling of prediction errors, and entropy coding of prediction errors. The compression ratios obtained by using CALIC with and without different BAR schemes are depicted in Fig. 12. A significant improvement in compression ratio is seen by using both BAR scheme with CALIC.

JPEG-LS with BAR: The ISO/IEC working group released a new standard for the lossless/ near-lossless compression of continuous-tone images in 1999, popularly known as JPEG-LS (ISO/IEC 1999). It has a low complexity and is based on the predictive coding technique. Near-lossless compression is controlled through an integer threshold representing the maximum

permissible absolute difference between each original pixel value and its decompressed value. The JPEG-LS encoder is composed of four main stages (Weinberger et al. 2000): prediction, context modeling, error encoding, and run mode, as depicted in Fig. 13. Figure 14 shows the compression ratios of JPEG-LS with and without the BAR preprocessing scheme applied along spectral and/or spatial dimension on the ten granules. It is seen that the combination of BAR+JPEG-LS significantly outperforms JPEG-LS applied alone.

4.3 Projection-based schemes

Lossless PCA: The Principal Component Analysis transform (PCA) or the Karhunen-Loève transform (KLT) has long been used in applications pertaining to hyperspectral images such as feature extraction, dimensionality reduction, and pattern recognition (Chang et al. 1999). PCA has also been used for lossy compression of hyperspectral imager data (Canta et al. 1998; Hoffman et al. 1994; Lee et al. 2000). We investigated PCA for lossless compression of the ultraspectral sounder data. PCA is a linear transform that constructs an orthogonal basis on which the data is projected. The data is simultaneously decorrelated by diagonalization of the data covariance matrix. The advantage of using PCA is that it gives the smallest average error when approximating a data set by its projection on an orthogonal basis (Mallat 1999). To ensure lossless compression of the ultraspectral sounder data, the error residuals are rounded and entropy-coded. The compression ratios of the ten granules using lossless PCA with 60 PC's are shown in Table 4.

Optimized Orthogonal Matching Pursuit based Linear Prediction: Linear prediction has been successfully used for lossless compression of ultraspectral sounder data (Huang et al. 2004a, Huang et al. 2005a). To find the optimal spectral predictors for each channel, we investigated the optimized orthogonal matching pursuit (OOMP) algorithm (Rebello-Neira et al. 2002). Matching pursuit (MP) represents any signal as a linear combination of basis signals, called *atoms*, chosen from an over-complete basis set, called the *dictionary*, to minimize the Euclidean distance between the original signal and its approximation (Rebello-Neira et al. 2002; Mallat et al. 1993). The OOMP selection criterion for the atoms can be implemented using the well-known Gram-Schmidt technique (Golub et al. 1996). For ultraspectral sounder data compression, each spatial frame is considered a vector that is predicted by atoms chosen using the OOMP algorithm. The selection of atoms for each channel proceeds iteratively, with the dictionary for each channel consisting of all channels that have been previously predicted. After linear prediction, the prediction error is entropy coded using an adaptive arithmetic coder. Table 5 shows the compression ratios achieved by LP using OOMP with 40 predictors for each channel.

4.4 Clustering-based schemes

Vector Quantization (VQ) (Gray 1984) has been used for hyperspectral imager data compression (Abousleman et al. 1997; Motta et al. 2003). To reduce the computational burden for ultraspectral sounder data compression, Predictive Partitioned VQ (PPVQ) was proposed by Huang et al. (2004a). This scheme falls under the category of predictive vector quantization (Cuperman et al. 1982; Gersho et al. 1992). An open-loop design methodology is used such that the predictor is designed independently of the VQ codebooks. The PPVQ scheme consists of four steps: linear prediction, channel partitioning, vector quantization, and entropy coding. Huang et al. (2005a) also developed a fast precomputed vector quantization (FPVQ) scheme with optimal bit allocation. Unlike previous bit allocation algorithms (Riskin 1991; Cuperman 1993) that may yield sub-optimal solutions, the proposed bit allocation algorithm guarantees the minimum of the cost function under the constraint of a given total bit rate.

The FPVQ scheme consists of five steps: linear prediction, bit-depth partitioning, vector quantization with precomputed codebooks, optimal bit allocation, and entropy coding. After linear prediction, channels with the same bit-depth of prediction error are assigned to the same partition for reducing the computational burden. To avoid the costly online codebook generation from the Linde-Buzo-Gray (LBG) algorithm (Linde et al. 1980), precomputed VQ codebooks are applied to each partition independently. The linear prediction error of each channel is close to a Gaussian distribution with a different standard deviation. Thus, only codebooks with 2^m codewords for 2^k -dimensional normalized Gaussian distributions are precomputed via the LBG algorithm. The channels in the i -th partition are thus sub-partitioned as a linear combination of 2^k . The number of bits for representing the quantization errors within each sub-partition depends on the sub-partition size and its codebook size. The minimization problem can be formulated as

$$f(b_{ij}^*) = \arg \min_{b_{ij}} \sum_{i=1}^{n_d} \sum_{j=1}^{m_{ib}} L_{ij}(b_{ij}) \quad (1)$$

subject to

$$\sum_{i=1}^{n_d} \sum_{j=1}^{m_{ib}} b_{ij} = n_b, \quad (2)$$

where

$$L_{ij}(b_{ij}) = -n_{ij} \sum_{k=1}^{n_p(b_{ij})} p_k(b_{ij}) \log_2 p_k(b_{ij}) + \frac{n_{ij}}{m_{ij}} b_{ij} \quad (3)$$

is the expected total number of bits for the quantization errors in the i -th partition and the j -th sub-partition and for the quantization indices; b_{ij} is the codebook size in bits for the corresponding sub-partition; n_d the number of partitions; m_{ib} the number of sub-partitions in the i -th partition; n_b the total bits of all the codebooks; n_{ij} the

number of pixels within that sub-partition; n_p the number of distinct values of quantization errors, and p_k the occurrence probability of the k -th distinct value. Both n_p and p_k depend on the codebook size b_{ij} . For lossless compression, the distortion measure using the total bits for the quantization errors and the quantization indices appears to be superior to using the squared error measure. The new optimal bit assignment algorithm for finding the solution to Eq. (1) with the constraint Eq. (2) consists of the following steps:

Step 1) Set $b_{ij} = 1, \forall i, j$.

Step 2) Compute the marginal decrement $\Delta L_{ij} = L_{ij}(2) - L_{ij}(1), \forall i, j$.

Step 3) Find indices α, β for which $\Delta L_{\alpha\beta}(b_{\alpha\beta})$ is minimum.

Step 4) Set $b_{\alpha\beta} = b_{\alpha\beta} + 1$.

Step 5) Update $\Delta L_{\alpha\beta} = L_{\alpha\beta}(b_{\alpha\beta}) - L_{\alpha\beta}(b_{\alpha\beta} - 1)$.

Step 6) Repeat Steps 2-5 until $\sum_{i=1}^{n_d} \sum_{j=1}^{m_{ib}} b_{ij} = n_b$.

Step 7) Compute the next marginal decrement

$\Delta L_{ij}^* = L_{ij}(b_{ij} + 1) - L_{ij}(b_{ij}), \forall i, j$.

Step 8) Find $(\kappa, \lambda) = \arg \min_{(i,j)} \Delta L_{ij}^*(b_{ij})$ and

$(\nu, \theta) = \arg \max_{(i,j) \neq (\kappa, \lambda)} \Delta L_{ij}^*(b_{ij})$.

Step 9) If $\Delta L_{\kappa\lambda}^* < \Delta L_{\nu\theta}$, set $b_{\kappa\lambda} = b_{\kappa\lambda} + 1$,

$b_{\nu\theta} = b_{\nu\theta} - 1$, update $\Delta L_{\kappa\lambda}^* = L_{\kappa\lambda}(b_{\kappa\lambda}) - L_{\kappa\lambda}(b_{\kappa\lambda} - 1)$, and go to Step 8; else, STOP.

After the VQ stage, a context-based adaptive arithmetic coder (Witten et al. 1987) is used to encode the data quantization indices and quantization errors. The FPVQ scheme is fast in the sense that the online time-consuming codebook generation is avoided by use of precomputed codebooks.

For comparison with PPVQ and FPVQ, we also investigate the Differential Partitioned VQ (DPVQ) and Partitioned VQ (PVQ) schemes (Huang et al 2005c). In the DPVQ scheme, the spectral difference between successive neighboring channels is calculated. The rest of the steps viz. channel partitioning, vector quantization and entropy coding are the same as those used in the PPVQ scheme. In the PVQ scheme, channels are partitioned according to their original bit-depths, followed by vector quantization and entropy coding. Table 6 shows the compression ratios achieved by these schemes. As seen, PPVQ and FPVQ schemes significantly outperform DPVQ and PVQ.

5. SUMMARY

The compression of ultraspectral sounder data is preferred to be lossless or near-lossless to avoid potential degradation of the geophysical retrieval in the associated ill-posed problem. In this paper, a systematic study of lossless compression techniques for the next generation NOAA GOES-R Hyperspectral Environmental Suite is presented. The lossless compression results are obtained and compared from, a) transform-based b) prediction-based c) projection-based and d) clustering-based compression methods. Robust data preprocessing schemes (e.g. BAR, MST reordering) are also demonstrated to improve compression gains of existing state-of-the-art compression methods such as JPEG2000, 3D SPIHT, JPEG-LS, and CALIC.

Acknowledgement

This work is sponsored by NOAA under grant NA07EC0676, and has been prepared in support of the NOAA GOES-R data compression research group led by Roger Heymann of NOAA NESDIS Office of Systems Development and Tim Schmit of NOAA NESDIS Office of Research and Applications.

References

- Abousleman G. P., M. W. Marcellin, and B. R. Hunt, 1997: Hyperspectral image compression using entropy-constrained predictive trellis coded quantization, *IEEE Transactions on Image Processing*, 6 (4), 566-573.
- Aumann H. H., and L. Strow, 2001: AIRS, the first ultraspectral infrared sounder for operational weather forecasting, *Proceedings of IEEE Aerospace Conference*, 1683-1692.
- Bloom H. J., 2001: The Cross-track Infrared Sounder (CrIS): a sensor for operational meteorological remote sensing, *Proceedings of the 2001 International Geoscience and Remote Sensing Symposium*, 1341-1343.
- Canta G. R., and G. Poggi, 1998: Kronecker-product gain-shape vector quantization for multispectral and hyperspectral image coding, *IEEE Transactions on Image Processing*, 7 (5), 668-678.
- Chang C.-I., and Q. Du, 1999: Interference and noise-adjusted principal components analysis, *IEEE Transactions on Geoscience and Remote Sensing*, 37 (5), 2387-2396.
- Cheung K., C. Cheung, and L. Po, 1999: A novel multiwavelet-based integer transform for lossless image coding, *Proc. ICIP*, 444-447.

- Cormen T. H., C. E. Leiserson, R. L. Rivest, and C. Stein, 2001: *Introduction to Algorithms, 2nd Edition*, The MIT Press, 1180.
- Cuperman V., and A. Gersho, 1982: Adaptive differential vector coding of speech, *Conference Record GlobeCom 82*, 1092-1096.
- Cuperman V., 1993: Joint bit allocation and dimensions optimization for vector transform quantization, *IEEE Transactions on Information Theory*, 39 (1), 302–305.
- Dragotti P. L., G. Poggi, A. R. P. Ragozini, 2000: Compression of multispectral images by three-dimensional SPIHT algorithm, *IEEE Transactions on Geoscience and Remote Sensing*, 38 (1), 416-428.
- Gersho A., and R.M. Gray, 1992: *Vector Quantization and Signal Compression*. Norwell, Mass: Kluwer Academic.
- Golomb S. W., 1966: Run-length encodings, *IEEE Trans. Inf. Theory*, IT-12, 399-401.
- Golub G. H., and C. F. Van Loan, 1996: *Matrix Computations*, John Hopkins University Press.
- Hoffman R. N., and D. W. Johnson, 1994: Application of EOF's to multispectral imagery: data compression and noise detection for AVIRIS, *IEEE Transactions on Geoscience and Remote Sensing*, 32 (1), 25-34.
- Huang, B., W. L. Smith, H.-L. Huang, and H. M. Woolf, 2002: Comparison of linear forms of the radiative transfer equation with analytic Jacobians, *Applied Optics*, 41 (21), 4209-4219.
- Huang B., H.-L. Huang, H. Chen, A. Ahuja, K. Baggett, T. J. Schmit, and R. W. Heymann, 2003: Data compression studies for NOAA hyperspectral environmental suite using 3D integer wavelet transforms with 3D set partitioning in hierarchical trees, *SPIE Int. Symp. Remote Sensing Europe, Proc. of SPIE*, 5238, 255-265.
- Huang B., A. Ahuja, H.-L. Huang, T. J. Schmit, and R. W. Heymann, 2004a: Predictive partitioned vector quantization for hyperspectral sounder data compression, *SPIE Annual Meeting 2004, Proc. of SPIE*, 5548, 70-77.
- Huang B., A. Ahuja, H.-L. Huang, T. J. Schmit, and R. W. Heymann, 2004b: Lossless compression of 3D hyperspectral sounding data using context-based adaptive lossless image codec with Bias-Adjusted Reordering. *Optical Engineering*, 43 (9), 2071-2079.
- Huang B., A. Ahuja, H.-L. Huang, T. J. Schmit, and R. W. Heymann, 2004c: Effects of the starting channel for spectral reordering on the lossless compression of ultraspectral sounder data, *SPIE International Asia-Pacific Symposium, 8-11 November, Honolulu, Hawaii*.
- Huang B., A. Ahuja, H.-L. Huang, T. J. Schmit, and R. W. Heymann, 2005a: Fast precomputed VQ with optimal bit allocation for lossless compression of ultraspectral sounder data, *Proceedings of the 2005 IEEE Data Compression Conference*, 408-417.
- Huang B., A. Ahuja, H.-L. Huang, T. J. Schmit, and R. W. Heymann, 2005b: Current Status of ultraspectral sounder data compression, *SPIE Annual Meeting, San Diego, 31 July – 4 August 2005, Proc. SPIE*, 5889, 35-48.
- Huang B., A. Ahuja, H.-L. Huang, 2005c: *Lossless Compression of Ultraspectral Sounder Data, Hyperspectral Data Compression*, edited by G. Motta and J. Storer, Springer-Verlag.
- Huang B., A. Ahuja, H.-L. Huang, T. J. Schmit, and R. W. Heymann, 2005d: Ultraspectral sounder data compression using error-detecting reversible variable-length codes, *SPIE Annual Meeting, San Diego, 31 July – 4 August 2005, Proc. SPIE*, 5889, 167-176.
- Huffman D. A., 1952: A method for construction of minimum redundancy codes, *Proceedings of IRE*, 40, 1098-1101.
- ISO/IEC 14496-2, 1998: Final draft international standard: Information technology – Coding of audio-visual objects: Visual.
- ISO/IEC 14495-1 and ITU Recommendation T.87, 1999: Information Technology – lossless and near-lossless compression of continuous-tone still images.
- ISO/IEC 15444-1, 2000a: Information technology - JPEG2000 image coding system-part 1: Core coding system.
- ISO/IEC 15444-2, 2000b: Information technology - JPEG2000 image coding system: Extensions.
- ITU-T Recommendation H.263, 1995: Video coding for low bit rate communication.
- Lee H. S., N.-H. Younan, and R. L. King, 2000: Hyperspectral image cube compression combining JPEG 2000 and spectral decorrelation, *Proceedings of the IEEE International Geoscience and Remote Sensing Symposium (IGARSS)*, 6, 3317-3319.
- Kubasova O., P. Toivanen, J. Mielikainen, 2004: Lossless Compression of 3D Hyperspectral Sounding Data Via Statistical Image Characteristics, *WSEAS Transactions on Systems*, 3 (6), 2368-2373.
- Linde Y., A. Buzo, and R.M. Gray, 1980: An Algorithm for Vector Quantizer Design, *IEEE Trans. Commun.*, COM-28, 84-95.

- Mallat S. G., and Z. Zhang, 1993: Matching pursuits with time-frequency dictionaries, *IEEE Transactions on Signal Processing*, 41 (12), 3397-3415.
- Mallat S., 1999: *A wavelet tour of signal processing*. Elsevier Academic Press.
- Martin M. B., and A. E. Bell, 2001. New image compression techniques using multiwavelets and multiwavelet packets, *IEEE Transactions on Image Processing*, 10, 500–510.
- Motta G., F. Rizzo, and J. A. Storer, 2003: Compression of hyperspectral imagery, *Proceedings of the 2003 IEEE Data Compression Conference*, 333-342.
- Phulpin T., F. Cayla, G. Chalon, D. Diebel, and D. Schlüssel, 2002: IASI onboard Metop: Project status and scientific preparation, *12th Int. TOVS Study Conf., Lorne, Victoria, Australia*, 234-243.
- Rebello-Neira L., and D. Lowe, 2002: Optimized orthogonal matching pursuit approach, *IEEE Signal Processing Letters*, 9 (4), 137-140.
- Rice R. F., 1979: Some practical universal noiseless coding techniques, *Tech Rep. JPL-79-22*, Jet Propulsion Laboratory, Pasadena, CA.
- Riskin E. A., 1991: Optimal bit allocation via the generalized BFOS algorithm, *IEEE Transactions on Information Theory*, 37 (2), 400-402.
- Said A., and W. A. Pearlman, 1996: A new, fast, and efficient image codec based on set partitioning in hierarchical trees, *IEEE Transactions on Circuits and Systems for Video Technology*, 6 (3), 243-250.
- Said A., 2004: Introduction to Arithmetic coding theory and practice, *Hewlett-Packard Laboratories Report*, HPL-2004-76.
- Smith W. L., F. W. Harrison, D. E. Hinton, H. E. Revercomb, G. E. Bingham, R. Petersen, and J. C. Dodge, 2002: GIFTS - the precursor geostationary satellite component of the future earth observing system, *Proceedings of the 2002 International Geoscience and Remote Sensing Symposium*, 357-361.
- Takishima Y., M. Wada, and H. Murakami, 1995: Reversible variable length codes, *IEEE Transactions on Communications*, 43, 158-162.
- Tang X., S. Cho, and W.A. Pearlman, 2003: Comparison of 3D set partitioning methods in hyperspectral image compression featuring an improved 3D-SPIHT, *Proceedings of the 2003 IEEE Data Compression Conference*, 449.
- Tate S. R., 1997: Band ordering in lossless compression of multispectral images, *IEEE Transactions on Computers*, 46 (4), 477-483.
- Taubman D., 2000: High performance scalable image compression with EBCOT, *IEEE Transactions on Image Processing*, 9, 1158-1170.
- Taubman D., and M. Marcellin, 2002: *JPEG2000: Image Compression Fundamentals, Standards and Practice*. Kluwer Academic, Norwell.
- Toivanen P., O. Kubasova, and J. Mielikainen, 2005: Correlation-based band-ordering heuristic for lossless compression of hyperspectral sounder data, *IEEE Geoscience and Remote Sensing Letters*, 1 (1), 1-5.
- Weinberger M. J., G. Seroussi, and G. Sapiro, 2000: The LOCO-I lossless image compression algorithm: principles and standardization into JPEG-LS, *IEEE Transactions on Image Processing*, 9 (8), 1309-1324.
- Witten I. H., R. M. Neal, and J. C. Cleary, 1987: Arithmetic Coding for Data Compression, *Comm. ACM*, 30 (6), 520-541.
- Wu X., 1997: Lossless compression of continuous-tone images via context selection, quantization, and modeling, *IEEE Transactions on Image Processing*, 6 (5), 656–664.
- Yang K. M., L. Wu, and M. Mills, 1988: Fractal based image coding scheme using peano scan, *Proceedings of the 1988 International Symposium on Circuits and Systems*, 3, 2301-2304.

Granule 9	00:53:31 UTC	-12 H	(Pacific Ocean, Daytime)
Granule 16	01:35:31 UTC	+2 H	(Europe, Nighttime)
Granule 60	05:59:31 UTC	+7 H	(Asia, Daytime)
Granule 82	08:11:31 UTC	-5 H	(North America, Nighttime)
Granule 120	11:59:31 UTC	-10 H	(Antarctica, Nighttime)
Granule 126	12:35:31 UTC	-0 H	(Africa, Daytime)
Granule 129	12:53:31 UTC	-2 H	(Arctic, Daytime)
Granule 151	15:05:31 UTC	+11 H	(Australia, Nighttime)
Granule 182	18:11:31 UTC	+8 H	(Asia, Nighttime)
Granule 193	19:17:31 UTC	-7 H	(North America, Daytime)

Table 1. Ten selected AIRS granules for ultraspectral sounder data compression studies.

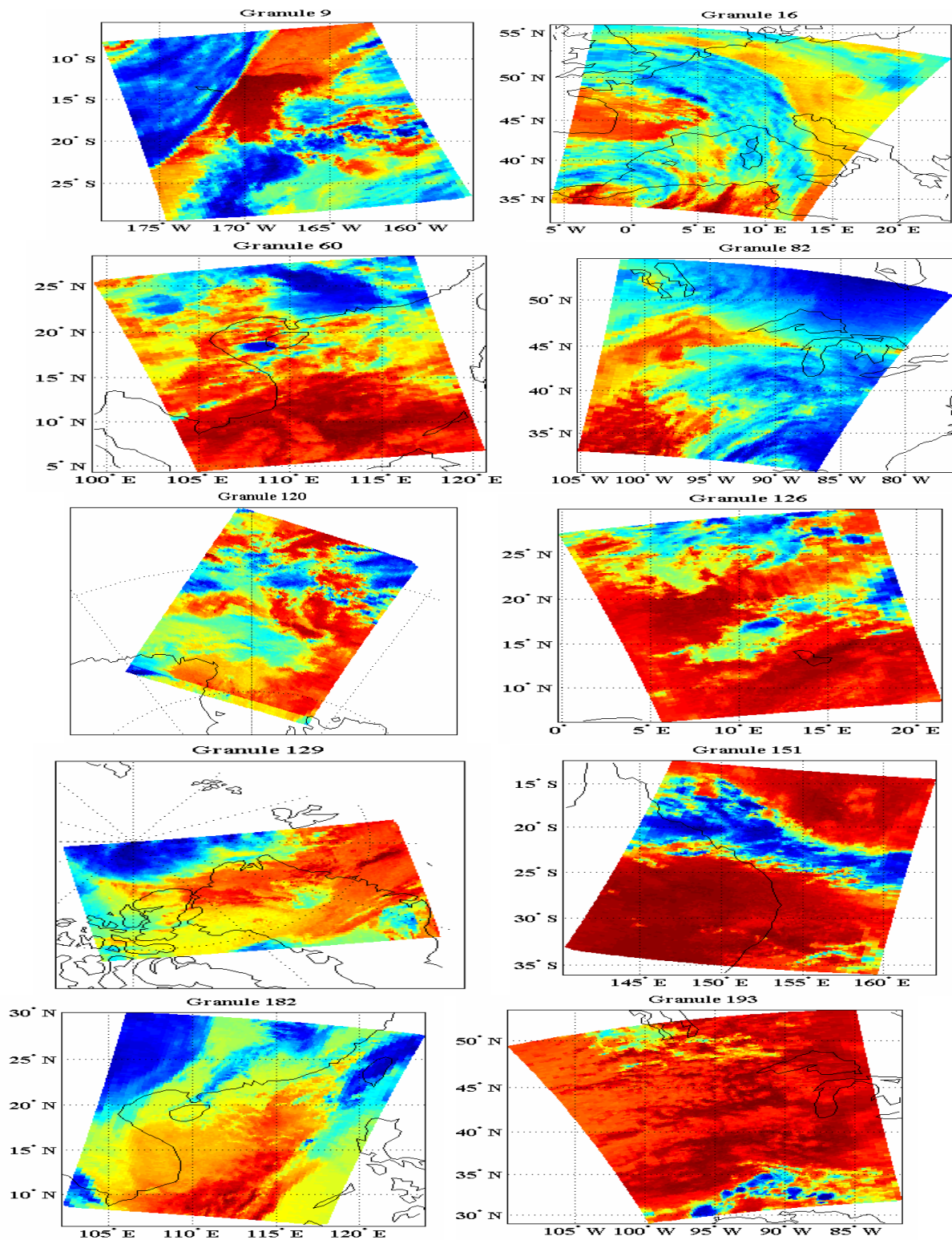


Figure 1. AIRS digital counts at wavenumber 800.01cm^{-1} for the 10 selected granules on March 2, 2004.

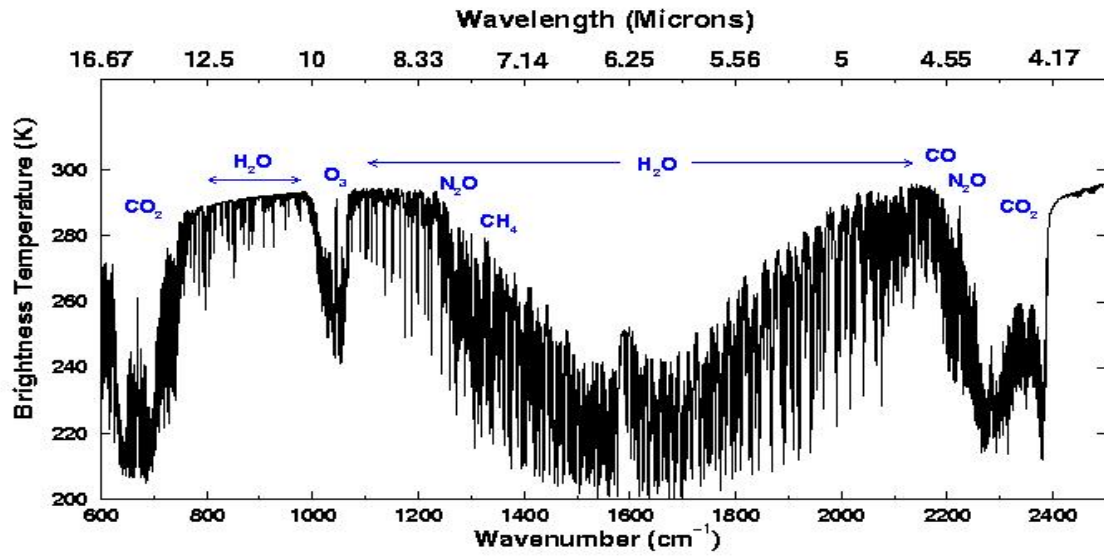


Figure 2. Dominant absorption gases in the infrared spectrum.

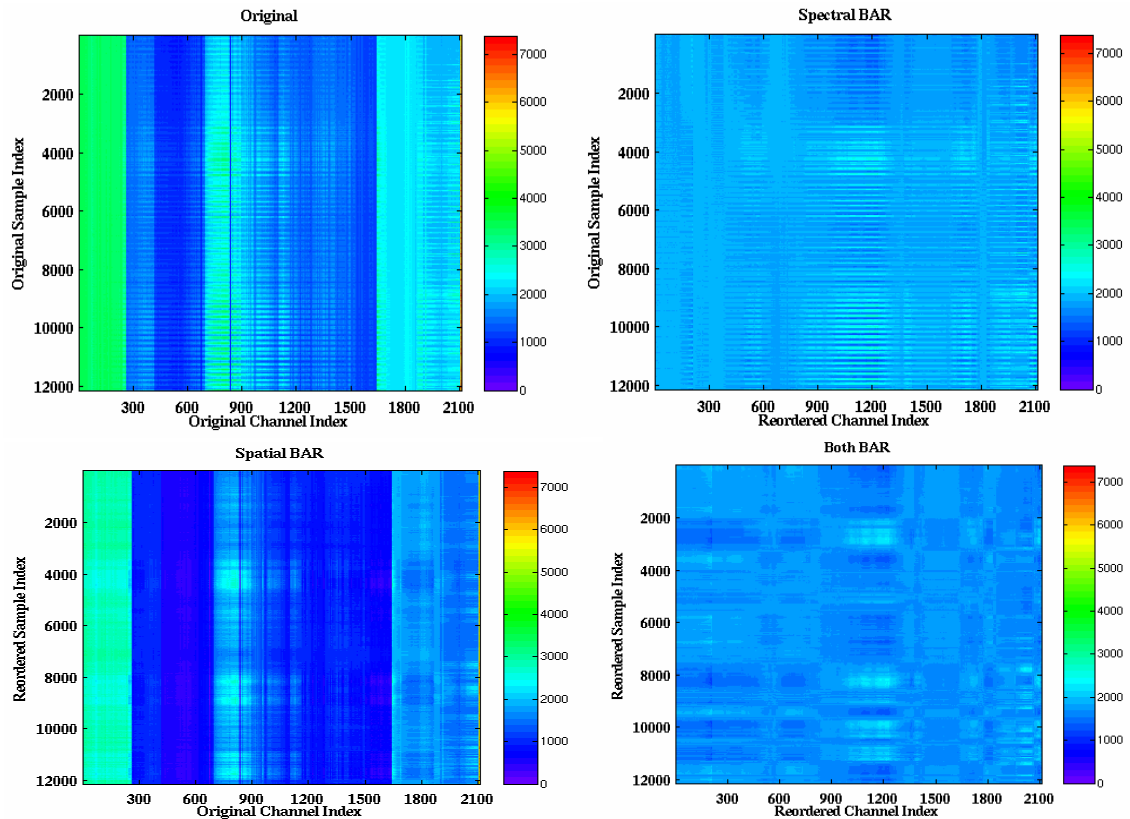


Figure 3. Example of 2D data distribution (a) of the original granule (b) after applying spectral BAR (c) after applying spatial BAR (d) after applying spectral BAR followed by spatial BAR.

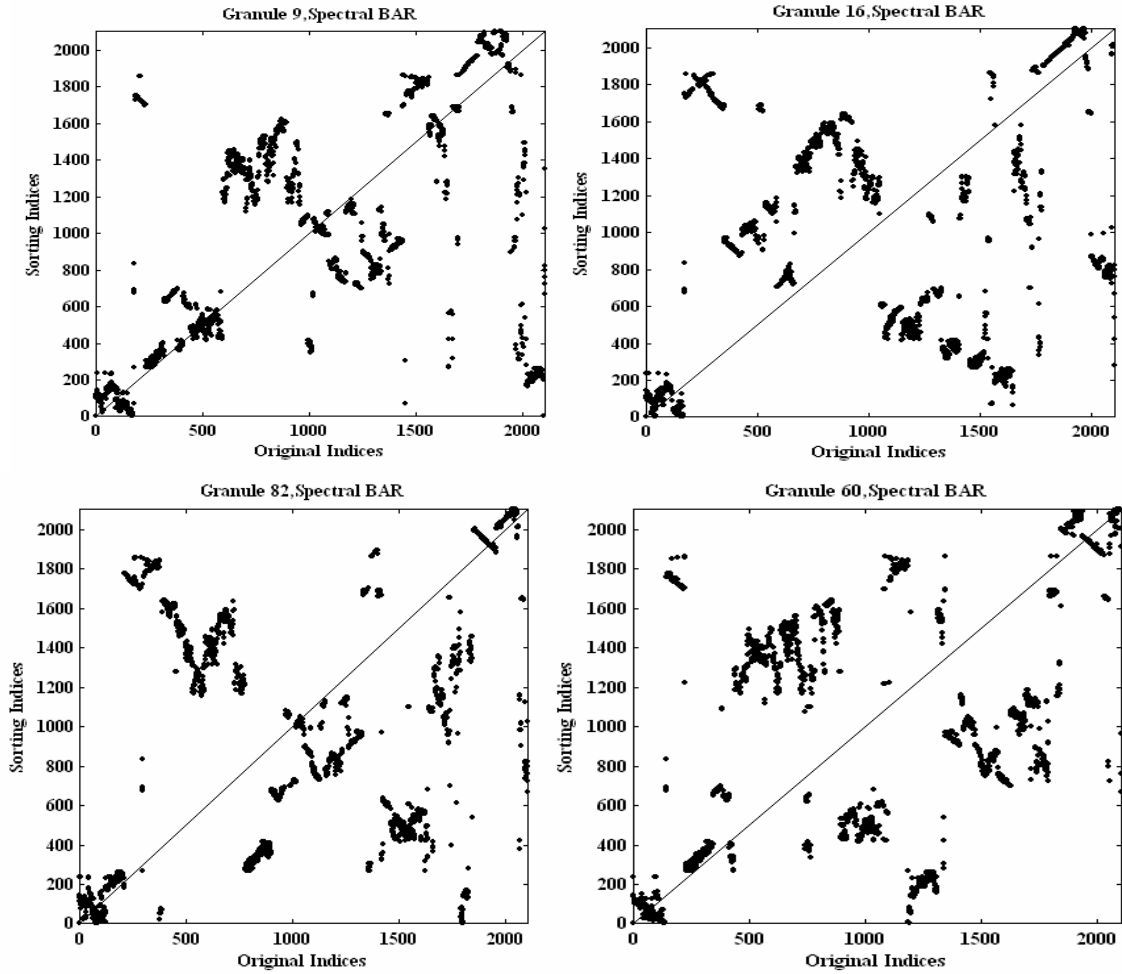


Figure 4. Spectral BAR sorting indices for various AIRS digital counts granules.

Granule	9	16	60	82	120	126	129	151	182	193	Average
MST+Context-free AC	2.57	2.73	2.42	2.75	2.58	2.44	2.73	2.34	2.35	2.49	2.54
BAR+Context-free AC	2.44	2.58	2.30	2.60	2.44	2.32	2.59	2.22	2.24	2.36	2.41
MST+Context-based AC	2.76	2.76	2.62	2.68	2.68	2.64	2.75	2.63	2.58	2.64	2.67
BAR+Context-based AC	2.68	2.80	2.66	2.81	2.61	2.63	2.83	2.64	2.60	2.64	2.69

Table 2. Compression ratios using MST reordering and BAR followed by arithmetic coding for 10 tested granules.

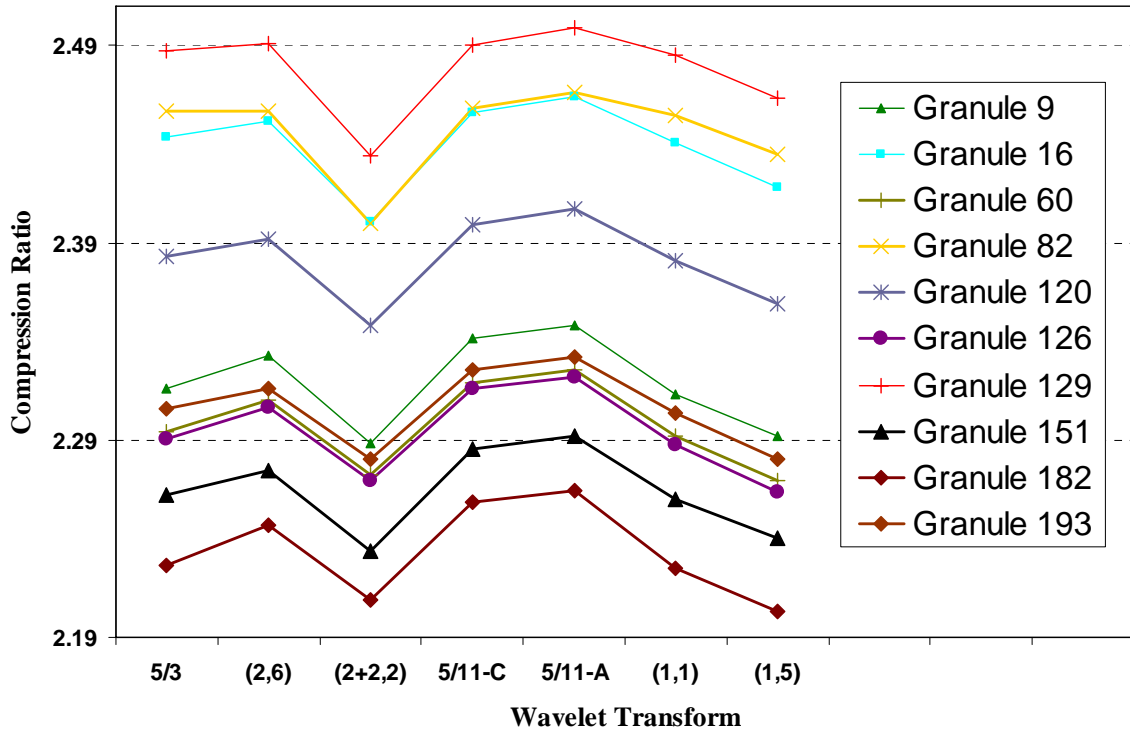


Figure 5. Compression ratios of ten granules using 3D SPIHT with various wavelet transforms.

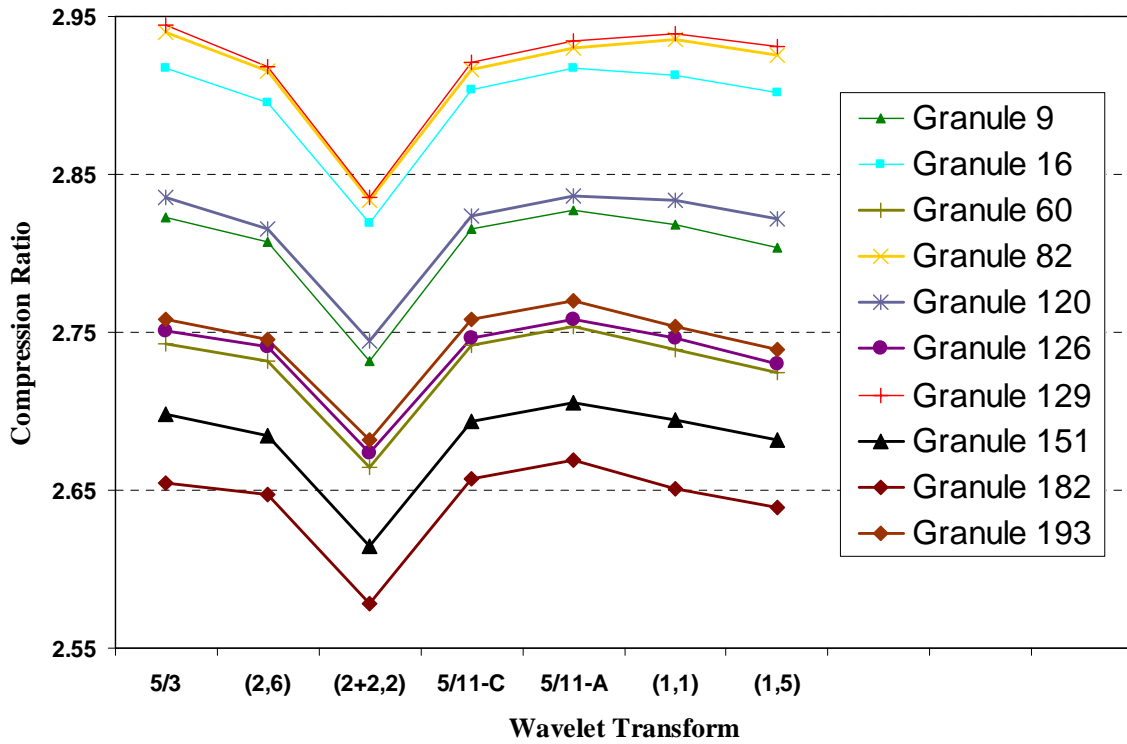


Figure 6. Compression ratios of ten granules using spectral BAR and 3D SPIHT with various wavelet transforms.

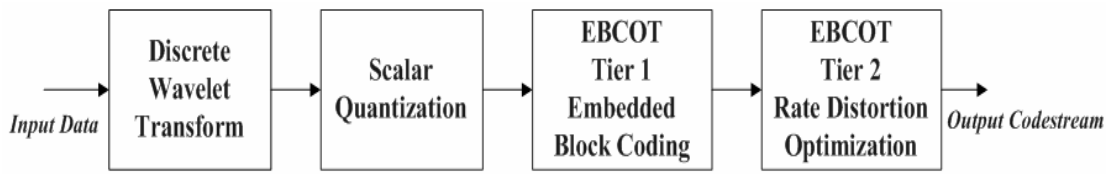


Figure 7. JPEG2000 encoder functional block diagram.

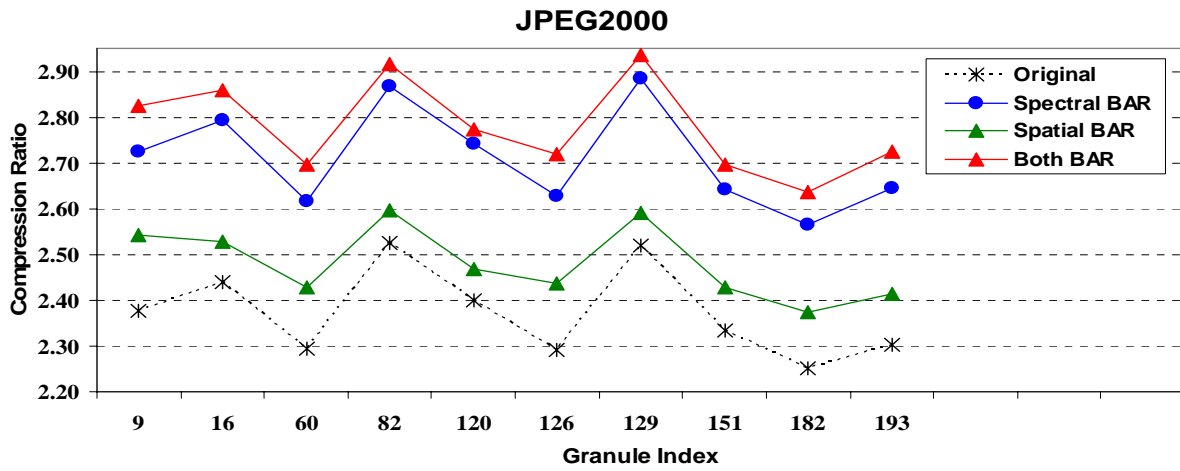


Figure 8. Compression ratios for JPEG2000 with and without BAR for ten tested granules.

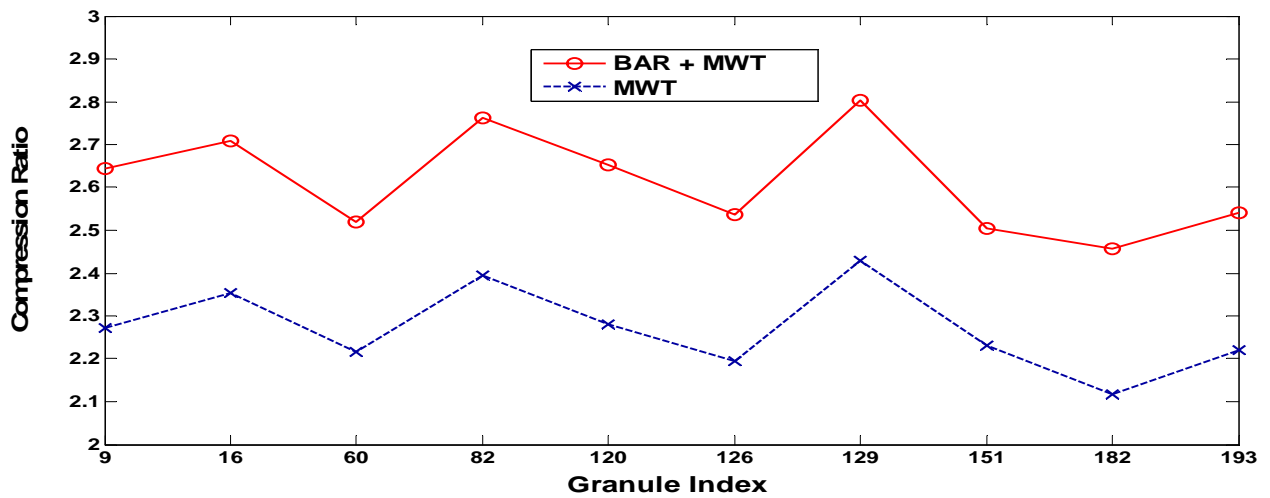
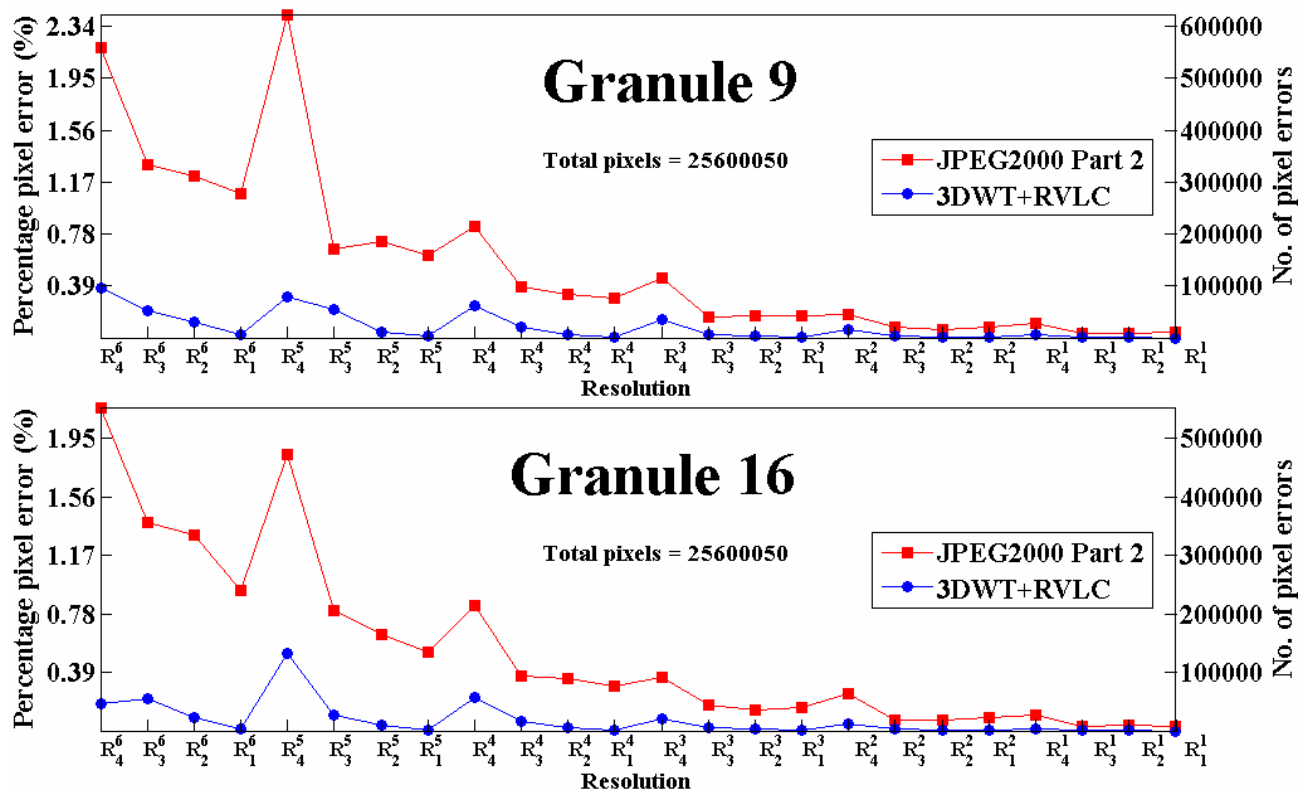
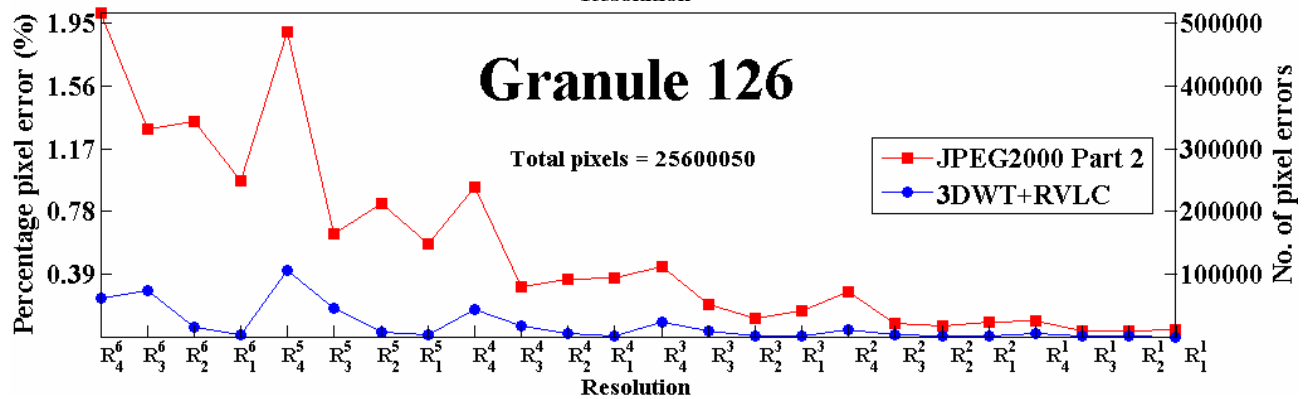
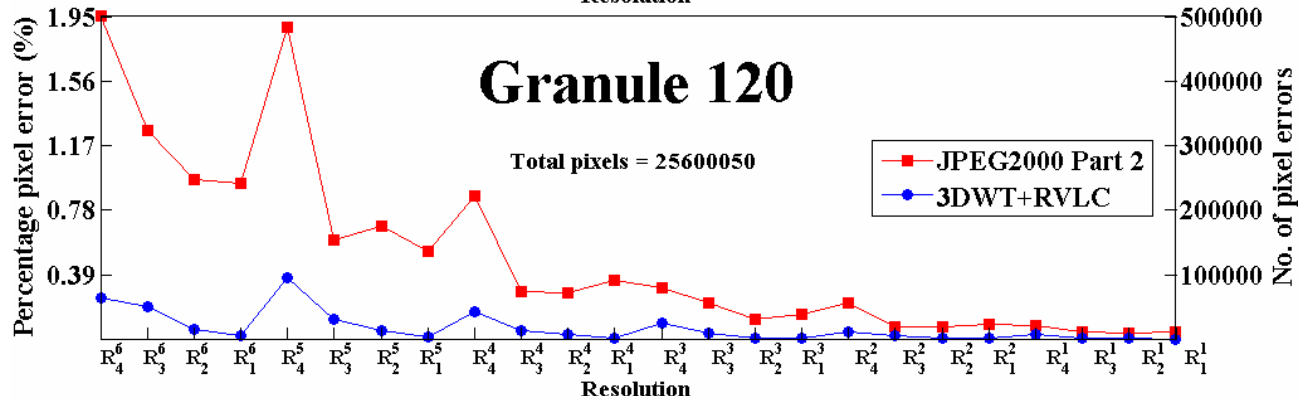
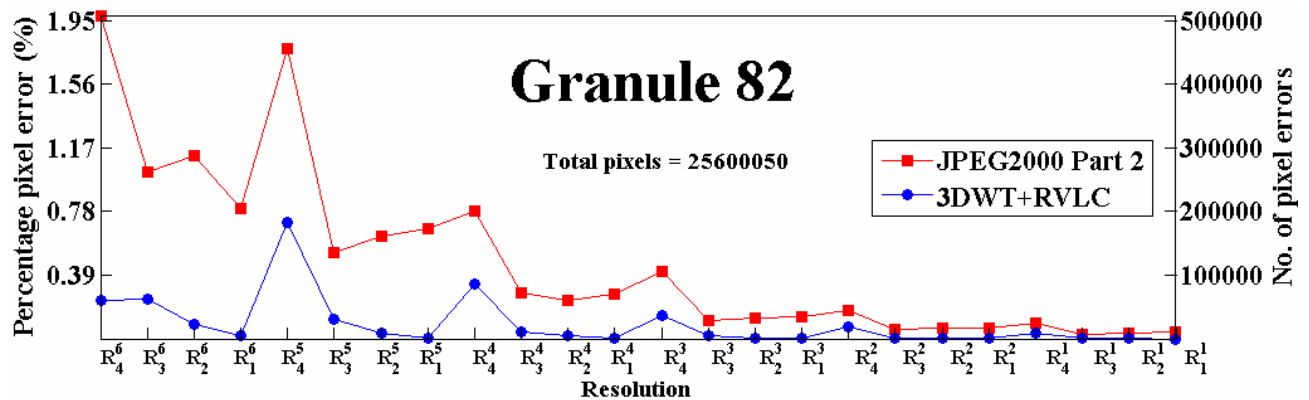
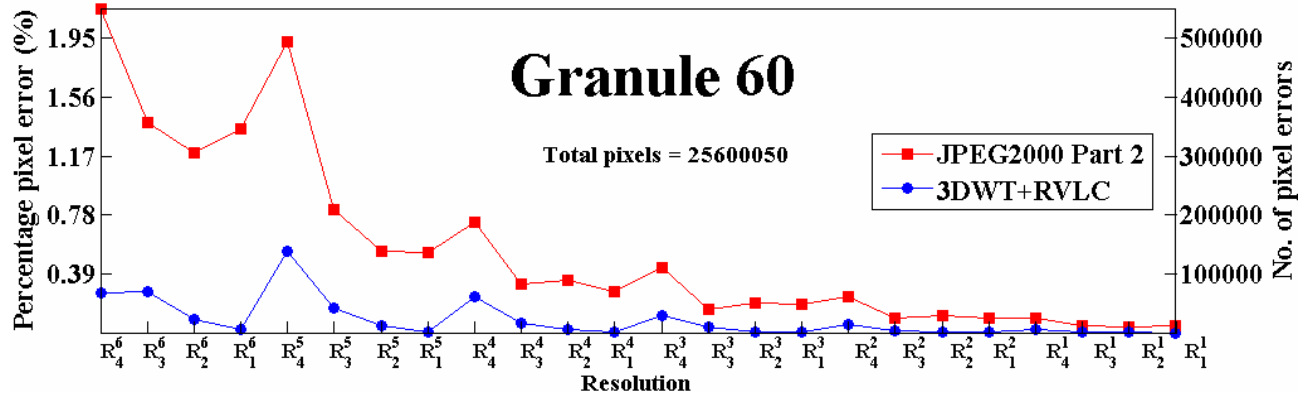


Figure 9. Compression ratios for multiwavelet (MWT) compression with and without BAR preprocessing.

Granules	JPEG2000 Part 2	3DWT+RVLC
9	2.63	2.53
16	2.71	2.60
60	2.51	2.40
82	2.80	2.67
120	2.62	2.52
126	2.51	2.40
129	2.82	2.70
151	2.55	2.46
182	2.52	2.41
193	2.51	2.39
Average	2.62	2.51

Table 3. Compression ratios of JPEG2000 Part 2 and 3DWT+RVLC for ten tested granules.





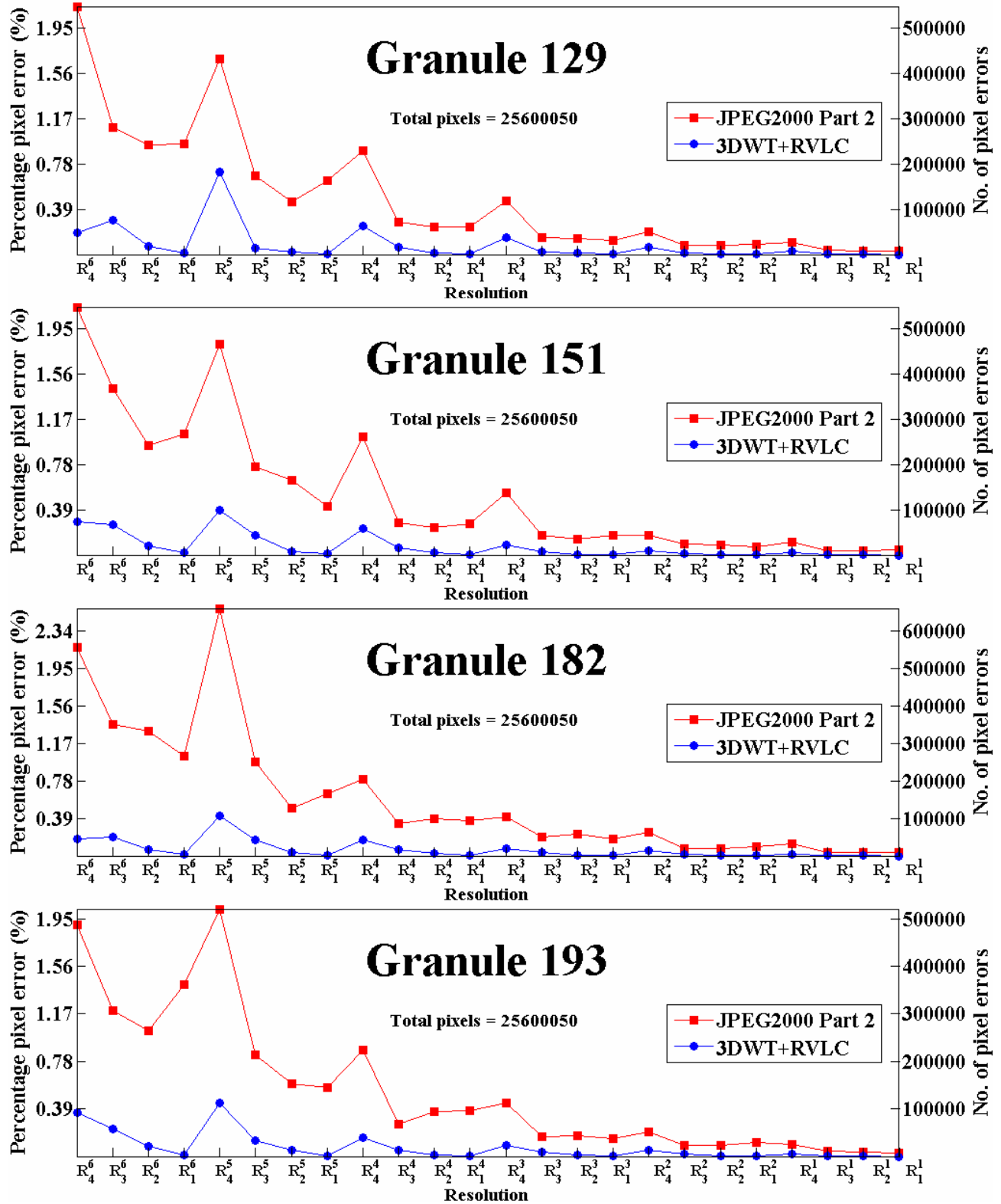


Figure 10. Average number of pixel errors for 30 events of single bit-error corruption in 24 resolutions of all the ten tested granules.

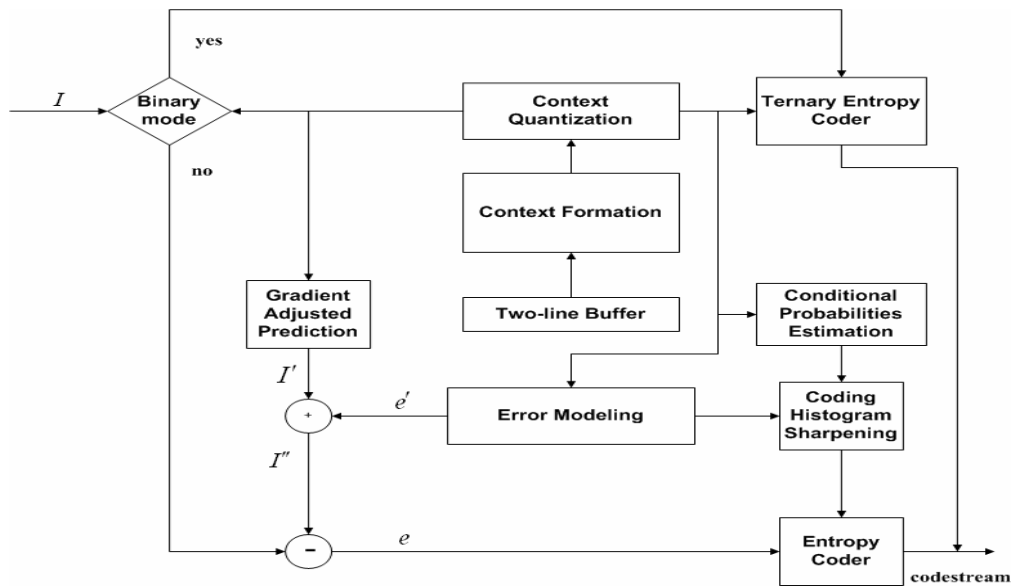


Figure 11. Schematic description of CALIC's encoder.

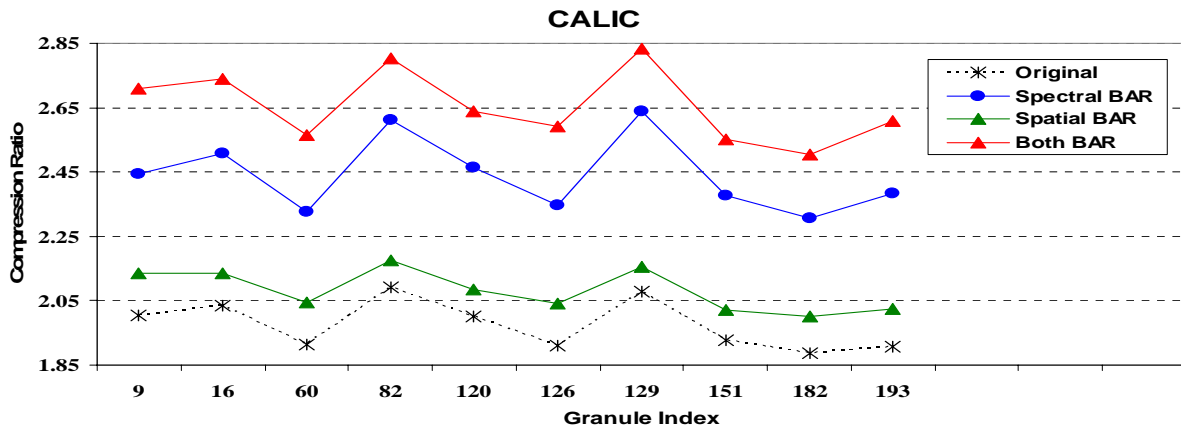


Figure 12. Compression ratios for CALIC with and without BAR for ten tested granules.

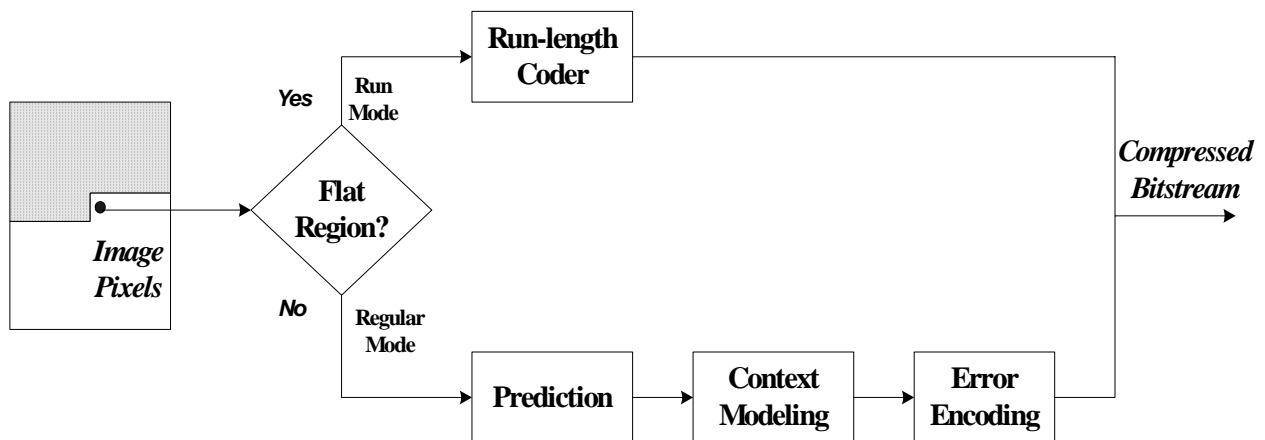


Figure 13. JPEG-LS encoder block diagram.

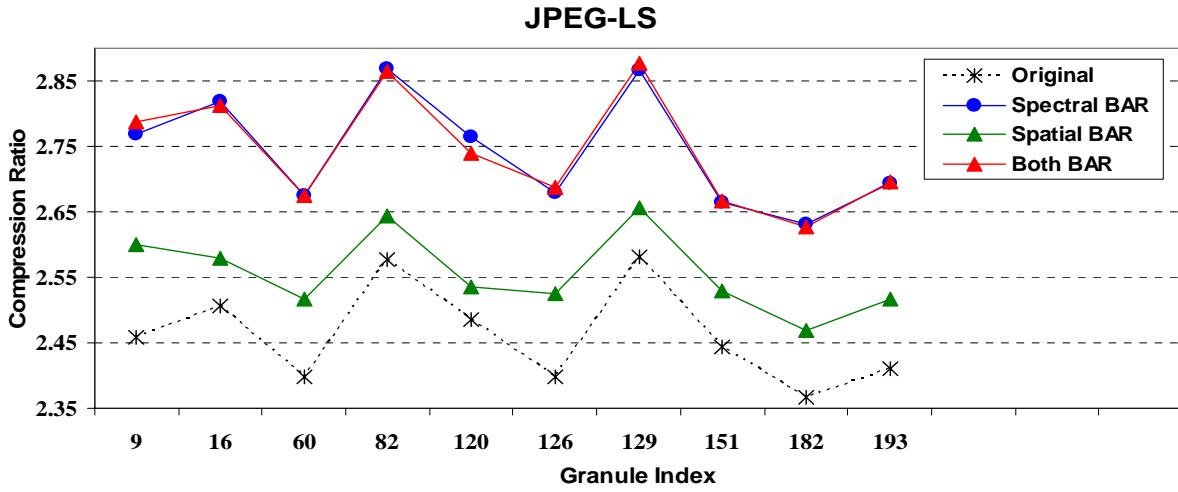


Figure 14. Compression ratios for JPEG-LS with and without BAR for ten tested granules.

Granule	9	16	60	82	120	126	129	151	182	193	Average
PCA	3.19	3.19	3.18	3.20	3.16	3.17	3.22	3.14	3.10	3.16	3.17

Table 4. Compression ratios using Lossless PCA with 60 eigenvectors for ten tested granules.

Granule	9	16	60	82	120	126	129	151	182	193	Average
OOMP-LP	3.21	3.30	2.78	3.11	3.26	2.81	2.81	2.79	2.74	3.33	3.01

Table 5. Compression ratios for OOMP-LP for ten tested granules.

Granule	PVQ	DPVQ	PPVQ	FPVQ
9	2.23	2.85	3.35	3.35
16	2.25	2.88	3.36	3.36
60	2.01	2.75	3.30	3.30
82	2.37	2.94	3.39	3.38
120	2.13	2.80	3.31	3.31
126	2.07	2.76	3.29	3.29
129	2.38	2.91	3.38	3.38
151	2.03	2.73	3.26	3.26
182	1.96	2.64	3.22	3.22
193	2.04	2.73	3.27	3.28
Average	2.15	2.80	3.31	3.31

Table 6. Compression ratios for partitioned VQ, DPVQ, and PPVQ on ten tested granules.